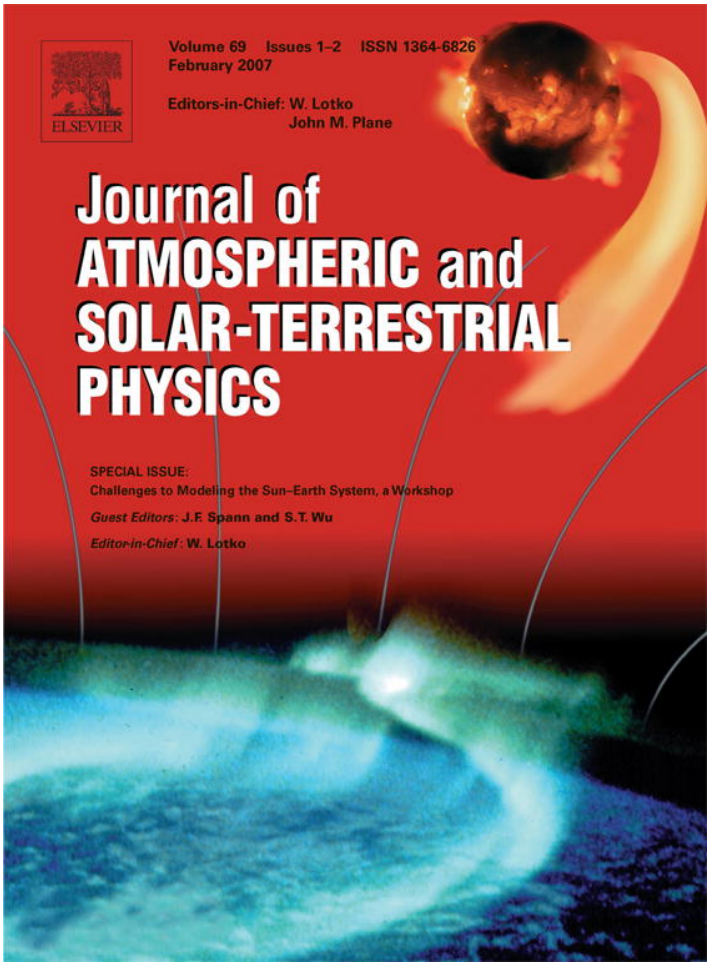

ELSEVIER

Journal of Atmospheric and Solar-Terrestrial Physics 69 (2007) 142–150

Journal of ATMOSPHERIC AND SOLAR-TERRESTRIAL PHYSICS

www.elsevier.com/locate/jastp

Strong pitch-angle diffusion of ring current ions in geomagnetic storm-associated conditions

G.V. Khazanov*, K.V. Gamayunov, D.L. Gallagher, J.F. Spann

NASA Marshall Space Flight Center, Huntsville, AL 35805, USA

Received 25 May 2005; accepted 24 July 2006
Available online 1 December 2006

Abstract

Do electromagnetic ion cyclotron waves cause strong pitch-angle diffusion of the ring current (RC) ions? This question is the primary motivation of this paper and has been affirmatively answered from the theoretical point of view. The materials that are presented in the Results section show clear evidence that strong pitch-angle diffusion takes place in the inner magnetosphere indicating an important role of the wave–particle interaction in the magnetospheric RC formation.

Keywords: Ring current; Wave–particle interaction; Strong pitch-angle diffusion; Numerical modeling

1. Introduction

Kennel and Petschek (1966) introduced the concept of strong pitch-angle diffusion to explain an observed >40 keV electron loss cone pitch-angle profile measured onboard the Injun 3 satellite (O'Brien, 1964). It is also believed that several geomagnetic storm-associated phenomena (e.g., ring current (RC) and relativistic electron formations, auroral precipitation) are actually observed to approximate the limit of strong pitch-angle diffusion (see Schulz and Lanzerotti (1974) and references therein).

In this paper, we focus on analysis of the electromagnetic ion cyclotron (EMIC) wave induced strong pitch-angle diffusion of the terrestrial RC during geomagnetic storm-associated conditions. To our knowledge, the first magnetospheric observations near the equatorial plane indicating strong proton pitch-angle diffusion are those published by Walt and Voss (2001, 2004) based on in situ measurements by the polar source/loss-cone energetic particle spectrometer (SEPS) (Blake et al., 1995). They presented high angular resolution measurements of 155 keV protons made during five magnetic storms in the last half of 1998. However, in only one case of strong pitch-angle scattering, the fluxes were isotropic for equatorial pitch angles less than 25°.

Walt and Voss (2001, 2004) presented a comprehensive analysis of their measurements and discussed all the known processes that can remove RC ions from the inner magnetosphere. Among them are charge-exchange collisions (Smith et al., 1976), collisional energy loss and scattering (Fok et al., 1991; Jordanova et al., 1996) convection into the atmosphere or through the dayside magnetopause

*Corresponding author. Tel.: +1 256 961 7517; fax: +1 256 961 7215.
E-mail address: george.khazanov@msfc.nasa.gov (G.V. Khazanov).

1364-6826/$ - see front matter
doi:10.1016/j.jastp.2006.07.010

(Kozyra et al., 1998; Liemohn et al., 1999), scattering into the loss cone by EMIC waves (Cornwall et al., 1970; Jordanova et al., 2001; Khazanov et al., 2002), and scattering by field-line curvature (Sergeev et al., 1983; Anderson et al., 1997).

In their latest paper, Walt and Voss (2004) expressed that the wave–particle scattering process is the most difficult to describe quantitatively, requiring knowledge of the particle anisotropy, of the cold plasma density, of the convective growth rate of the waves as they propagate through the magnetosphere, and of the resonant particle interaction with the wave fields. They also noted that in some theoretical RC models the wave–particle scattering process is greatly simplified and therefore does not predict the strong pitch-angle diffusion postulated by Cornwall et al. (1970) and observed by others (Hauge and Soraas, 1975; Soraas et al., 1999; Walt and Voss, 2001; Yahnina et al., 2000).

It should be noted that most of these above-cited measurements (except by Walt and Voss (2001, 2004)) were made at lower altitudes where the loss cone is large so that even moderate angular resolution instruments can separate trapped from precipitating particles. However, it would be difficult to evaluate the scattering processes that could be responsible for such pitch-angle distributions. To our knowledge, the only observations near the equatorial plane, giving evidence of proton pitch-angle diffusion related to EMIC waves, are those published by Erlandson and Ukhorskiy (2001). They considered protons with energies $E<17\,\mathrm{keV}$ and found the presence of this population consistent with simultaneously measured EMIC waves. However, the results of their study did not confirm that strong pith-angle diffusion of RC protons takes place even for relatively large amplitude of EMIC waves.

Do EMIC waves cause the strong pitch-angle diffusion of RC ions? At this point, there are no experimental or rigorous theoretical self-consistent studies that conclusively answer this question. In this paper, from theoretical point of view, we address the issue of RC proton strong pitch-angle diffusion and associated EMIC wave generation during different phases of the May 1–7, 1998 geomagnetic storm. This analysis is based on our newly developed self-consistent model of magnetospheric RC interacting with EMIC waves (Khazanov et al., 2003a).

2. Model

It is well known that the effects of EMIC waves on RC ion dynamics strongly depend on particle/wave characteristics such as the ion phase space distribution function, frequency, wave-normal angle, wave energy, and the form of wave spectral energy density. All of these characteristics should be properly determined by the wave–ion evolution itself. So to quantify the EMIC wave effects on RC ion dynamics, a self-consistent theoretical description of ions and waves should be employed in all RC studies. Here we present a short description of such self-consistent theoretical model that was developed by Khazanov et al. (2002, 2003a) and used in this particular study.

We simulate RC dynamics by solving the bounce-averaged kinetic equation for the phase space distribution function, Q, of the RC species,

$$\frac{\partial Q}{\partial t}+\frac{1}{R_o^2}\frac{\partial}{\partial R_o}\left(R_o^2\left\langle\frac{dR_0}{dt}\right\rangle Q\right)+\frac{\partial}{\partial\varphi}\left(\left\langle\frac{d\varphi}{dt}\right\rangle Q\right)+\frac{1}{\sqrt{E}}\frac{\partial}{\partial E}\left(\sqrt{E}\left\langle\frac{dE}{dt}\right\rangle Q\right)+\frac{1}{h(\mu_o)\mu_o}\frac{\partial}{\partial\mu_o}\left(h(\mu_o)\mu_o\left\langle\frac{d\mu_0}{dt}\right\rangle Q\right)=\left\langle\frac{\delta Q}{\delta t}\right\rangle_{\mathrm{collis}} \quad (1)$$

as a function of position in the magnetic equatorial plane (R_0,φ); kinetic energy and the cosine of the equatorial pitch angle (E,μ_0); and time t. In the left-hand side of this equation all of the bounce-averaged drift velocities are denoted as $\langle\ldots\rangle$. The term on the right-hand side of Eq. (1) includes losses from charge exchange, Coulomb collisions, ion–wave scattering, and precipitation at low altitudes. Loss through the dayside magnetopause is taken into account, allowing free outflow of RC ions from the simulation domain. (For more details regarding Eq. (1), see Jordanova et al. (1997); Khazanov et al. (2003a); and references therein].) The ion–wave collisional term, included in the right-hand side of Eq. (1), is a function of the EMIC wave power spectral density (see (Lyons and Williams, 1984) for details) that may be obtained from the wave-kinetic equation. EMIC waves propagate along geomagnetic field lines and reflect at ionosphere altitudes, bouncing between conjugate ionospheres. By averaging the wave-kinetic equation over one period of "fast" wave bounce oscillations, we can obtain an equation to describe the "slow" evolution of wave

power spectral density. Following Bespalov and Trakhtengerts (1986), the equation can be presented as

$$\frac{\partial\left\langle B^2_{\omega,\theta}\right\rangle}{\partial t} = \left[\ln R + 2\oint \frac{\gamma}{v\mathrm{g}}\,\mathrm{d}s\right]\frac{\left\langle B^2_{\omega,\theta}\right\rangle}{\tau_{\mathrm{g}}}, \quad (2)$$

where $\left\langle \tilde{B}^2_{\omega,\theta}\right\rangle = \left\langle B^2(\omega,\theta,\varphi,R_0)\right\rangle$ is averaged over one wave bounce oscillation; ω is the wave frequency; and θ the angle between the external magnetic field line and the wave vector. Parameter R is the effective reflection coefficient from the ionosphere characterizing wave energy loss due to imperfect reflection. The local wave growth rate, $\gamma(\omega, \theta, \varphi, R_0, s)$, which depends on the phase space distribution function of the RC species, should be averaged over one bounce oscillation of the wave envelope. The factor $\tau_{\mathrm{g}}/2$ is the time of the group propagation of the wave signal between conjugate ionospheres, and v_{g} the wave group velocity. It should be noted that γ includes contribution not only from EMIC wave growth due to interaction with RC ions but also from EMIC damping due to absorption by the core plasma particles (i.e., γ may change its sign). The right-hand side of the kinetic Eq. (1) depends on EMIC wave energy density, and γ in Eq. (2) is determined by the phase space distribution function Q. The resulting system of Eqs. (1) and (2) gives a self-consistent description of interacting RC ions and EMIC waves in a quasi-linear approach. Additional details, as well as a numerical implementation for (1) and (2) are given in the paper by Khazanov et al. (2003a).

3. Case study

Our model is used to study the geomagnetic storm of May 1–7, 1998. The interplanetary configuration of 1–7 May 1998 consists of a coronal mass ejection (CME) interacting with a trailing faster stream (Farrugia, 2001). The CME drives an interplanetary shock observed by the instruments on the Wind spacecraft at ~2200 UT on 1 May. Two periods of a strongly negative north–south IMF component were observed: the first at ~0400 UT on 2 May and the second at ~0200 UT on 4 May. These caused a "double-dip" storm with a minimum Dst = −100 and −215 nT, respectively. The planetary Kp index reached maximum values of 7 and 9 at the times when the minimum Dst were recorded.

This was a very large storm in which the RC developed quite rapidly, so it is a good candidate for investigating EMIC wave generation. It is also a storm that has been previously studied by this group (Khazanov et al., 2002, 2003a), where the influence of self-consistently calculated ion cyclotron waves were examined (particularly the effects in the late recovery phase) as well as nonlinear coupling of EMIC and lower hybrid waves (Khazanov et al., 2004a). In this paper, as we point out above, the analysis focuses on answering the following question: Do EMIC waves cause strong pitch-angle diffusion of RC ions?

Magnetospheric ion composition plays an extremely important role in the formation of EMIC waves. Cold, heavy plasmaspheric ions can have profound effects on the generation and propagation of EMIC waves (Young et al., 1982; Gomberoff and Neira, 1983). The most notable new features, in comparison with the case of single ion thermal plasma, are the formation of stop bands above the heavy ion gyrofrequencies and additional wave modes that we have presented in our previous paper (Khazanov et al., 2003a). Kozyra et al. (1984) added hot heavy ion populations (He^+ and O^+) in the dispersion equation analysis. In many respects, hot heavy ions modify the wave growth in the same way as the cold population, however for the purposes of this study the hot heavy ion populations of He^+ and O^+ are not taken into account. The results presented below correspond to a multi-component thermal plasma consisting of electrons, 77% H^+, 20% He^+, and 3% O^+, and only include the He^+ -mode of EMIC waves. The results for the case of pure electron–proton thermal plasma also will be presented and discussed.

4. Results

Fig. 1 represents the case of multi-component cold plasma and shows scatter plots of RC proton energies and EMIC wave magnetic fields that correspond to strong pitch-angle diffusion during the geomagnetic storm period of May 2–7, 1998. In this figure, the different colors for plotted stars correspond to the different selection criteria that have been applied to numerically obtained data. The following criteria are used for this event in order to find strong pitch-angle diffusion cases:

$$f(\alpha = 0)/f(\alpha_{\mathrm{LC}}) \geqslant 0.9, \quad (3)$$

$$0.1 \leqslant f(\alpha = 0)/f(\alpha = \pi/2) < 0.2, \quad (4)$$

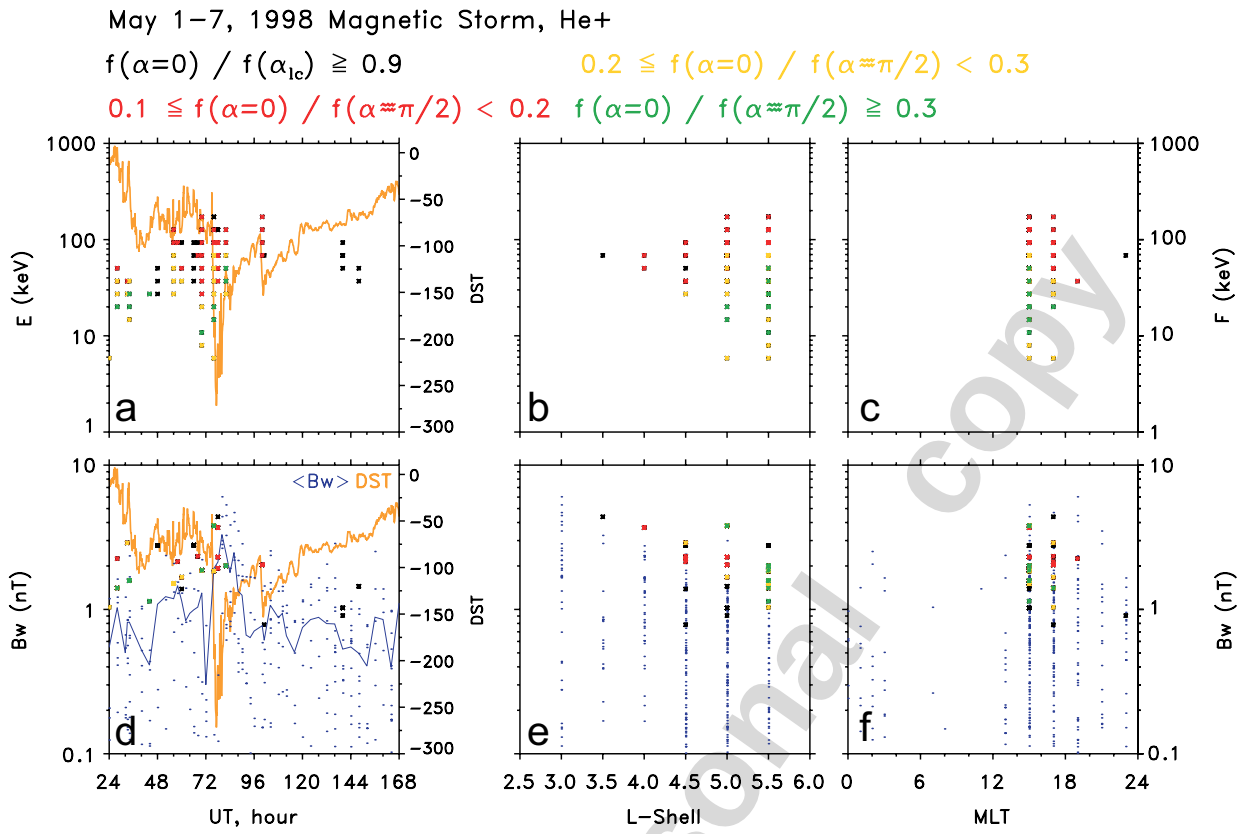

Fig. 1. Scatter plots of RC proton energies and EMIC wave magnetic fields for the case of multi-component thermal plasma versus UT, L shell, and MLT. The stars of different colors correspond to the different selection criteria (3)–(6) that are used. Black color corresponds to the cases when only criteria (3) is satisfied, red, yellow and green colors correspond to the cases when inequality (4), (5), or (6) is satisfied in combination with inequality (3), respectively. The only cases with loss cone RC proton fluxes that exceed $10^3\,\mathrm{cm^{-2}\,s^{-1}st^{-1}\,keV^{-1}}$ are presented. Dst index is also provided for convenience. In the second row, the simulated wave magnetic field which exceeds 0.1 nT is presented with blue small dots. Blue line in (d) represents an average EMIC wave magnetic field obtained by averaging over all spatial active zones for any particular time.

$$0.2 \leqslant f(\alpha = 0)/f(\alpha = \pi/2) < 0.3, \quad (5)$$

$$f(\alpha = 0)/f(\alpha = \pi/2) \geqslant 0.3. \quad (6)$$

Here $f(\alpha = 0)$, $f(\alpha_{LC} = 0)$ and $f(\alpha = \pi/0)$ are the RC proton fluxes at 0° pitch -angle, the loss cone boundary, and 90°, respectively. The inequality (3) allows us to select almost isotropic pitch-angle distributions in the loss cone. The inequalities (4)–(6) characterize the loss-cone fluxes as compared to the fluxes of trapped ions and characterize the strong pitch angle diffusion efficiency in the entire pitch-angle region. All stars that are plotted in Fig. 1 correspond to the cases when inequality (3) is satisfied and strong pitch-angle diffusion inside the loss cone takes place. The different star colors in this figure correspond to the cases when one of the inequalities (4), (5), or (6) is satisfied in combination with (3). The red color corresponds to the combination of (3) and (4), the yellow and green colors correspond to combinations of (3) and (5), and (3) and (6), respectively. In applying all these criteria to the analysis presented below only those cases with loss cone RC proton fluxes that exceed the value of $10^3\,\mathrm{cm^{-2}\,s^{-1}st^{-1}\,keV^{-1}}$ were taken into account.

The first row of Figs. 1(a)–(c) shows the energies of RC protons for which strong pitch-angle diffusion takes place. Fig. 1(a) shows all strong pitch-angle events that include all combinations with inequalities (3)–(6) during the entire geomagnetic storm of May 2–7, 1998. The Dst index is added in this plot in order to allow easier comparison within the various phases of the storm. Figs. 1(b) and (c) show the spatial location (in terms of L shells and MLT) where strong pitch-angle diffusion for different RC proton energies takes place.

The second row of Figs. 1(d)–(f) shows the magnetic field of EMIC waves that result from self-consistent coupling of Eqs. (1) and (2). The small blue dots represent all EMIC wave data when

magnetic intensity exceeds 0.1 nT. As in the first row, the Dst index is also included. The blue line in Fig. 1(d) is the average value of the magnetic field of EMIC waves during this storm, and is obtained by averaging over all spatial active zone locations for any particular time. Panels 1(e) and 1(f) show the spatial locations (in terms of L shell and MLT) of intense EMIC waves. We also added stars to these three plots indicating the appearance of strong pitch-angle diffusion for certain values of EMIC wave intensities. However, these stars do not give any information regarding what energies have been involved in the strong pith-angle diffusion process. Only by combining both rows of Fig. 1 can this detailed information be derived. The colors of the stars in the second row are based on different combinations of the (3)–(6) inequalities, as described above, and correspond to the most flatted transition between the trap zone and loss-cone populations, which takes place at any particular time.

It is instructive to compare the results presented in Fig. 1 with the corresponding ones that have been obtained in the case of pure electron–proton thermal plasma.These results are shown in Fig. 2. The presentation in Fig. 2 is in the same format as in Fig. 1 and exactly the same selection criteria (3)–(6) is applied for strong pitch-angle diffusion analysis. The similarities and differences between these figures are discussed below. In both cases during the main phase of the storm, the wave amplitudes of EMIC waves are greatly enhanced and the wave active region move to considerably lower L shells in the late evening MLT sector. (This behavior of EMIC waves is consistent with a great magnetic storm observed by the Freja double-probe electric field instrument presented by Braysy et al. (1998)). However there are very clear differences in the magnitude of these waves and their spatial distribution, which are dependent on the heavy ion magnetospheric content. The energy precipitation pattern, its spatial location, and the intensity of strong pitch-angle diffusion also have noticeable differences depending on the presence of heavy ions.

During the main and recovery phases of the geomagnetic storm of May 2–7, 1998 protons are often found in the loss cone. In many cases presented in Figs. 1(a) and 2(a) the pitch-angle distributions are nearly isotropic inside the loss cone, indicating that strong pith-angle diffusion is

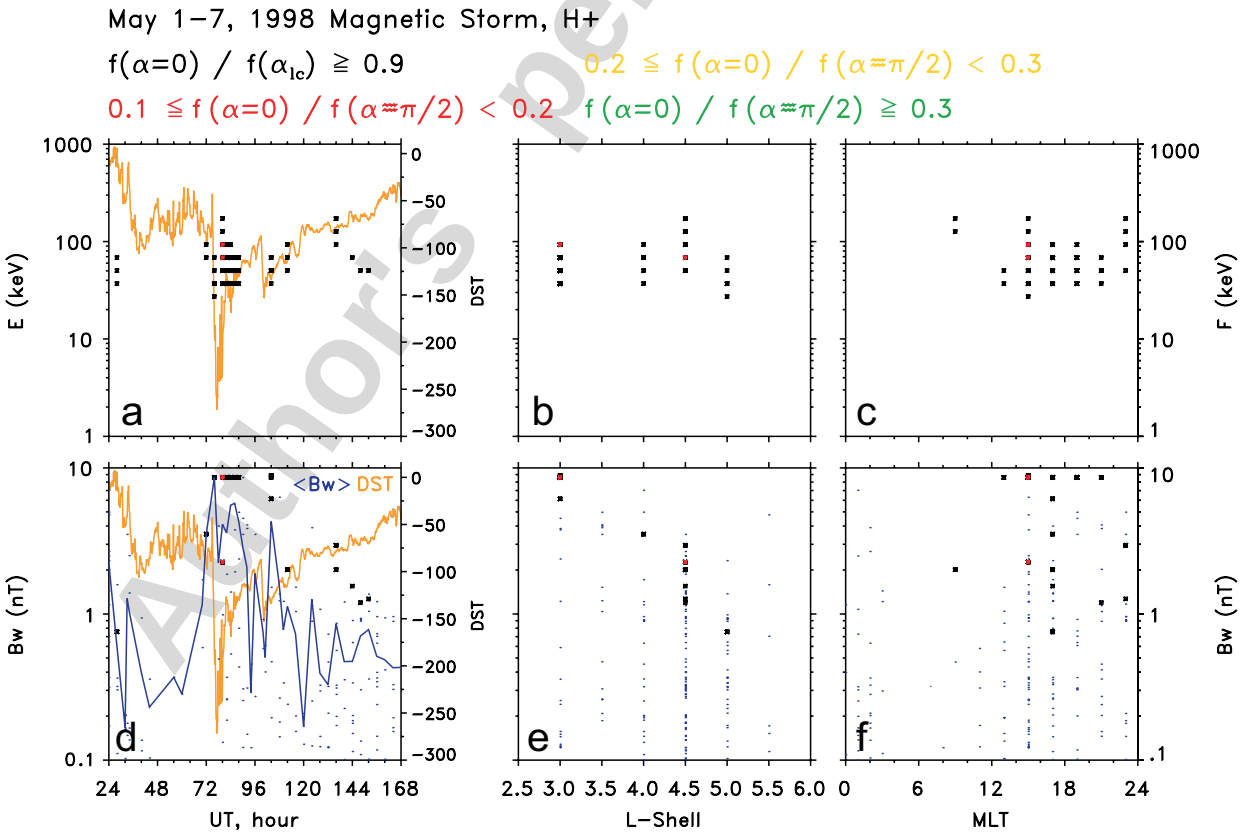

Fig. 2. As in Fig. 1, for the case of pure electron–proton thermal plasma.

taking place although the trapped flux at larger pitch-angle is always greater, to some degree, than precipitated fluxes (see different star colors and selection criteria definition (3)–(6)). Depending on the stage of the storm, plasma composition, and spatial location, the energy range that is involved in the strong diffusion process is very different. There are many stronger pitch-angle diffusion cases for multi-component (Fig. 1) than for single-ion (Fig. 2) plasmas. The presence of heavy ions in the magnetosphere leads to more cases with a flattening transition between the loss cone and trapped regions, which is also an indication of strong pitch-angle diffusion taking place in the trapped region.

Based on the results presented in Figs. 1 and 2, one can conclude that the highest power EMIC wave events are found in the dusk sector where the storm time RC is strongest. However depending on heavy ion magnetospheric composition, high power EMIC events can be found even in the day and night sectors. These results also suggest that low L shell ($3.0 < L < 5.5$) EMIC wave activity during this geomagnetic storm is strongly influenced by RC ion dynamics, and is in agreement with the data presented by Erlandson and Ukhorskiy (2001). The occurrence of strong pitch-angle diffusion is strongly correlated with the intensity of EMIC waves, while the heavy ion composition is extremely critical in the scattering efficiency of RC ions into the loss cone. In the case of multi-component thermal plasma, the mean intensity of EMIC waves in the main phase of the storm is weaker than for the case of a single-ion plasma. Nevertheless, in the presence of heavy ions the transition between the trapped and loss cone populations is much smoother for most of the cases where strong pitch-angle diffusion occurs (see color stars at the Figs. 1(a) and 2(a)).

Fig. 3 shows the pitch-angle distribution functions in the equatorial magnetosphere near the main phase of the geomagnetic storm for two of the strongest pitch-angle diffusion cases presented in Panels 1(a) and 2(a). Panel 3(a) illustrates the event when inequalities (3) and (6) are satisfied at UT = 82 h for an energy of 50 keV, L = 5.5, and MLT = 15 for the case of multi-component core plasma. Panel 3(b) presents the event when inequalities (3) and (4) are satisfied at UT = 80 h for an energy of 70 keV, $L = 4.5$, and MLT = 15 for the

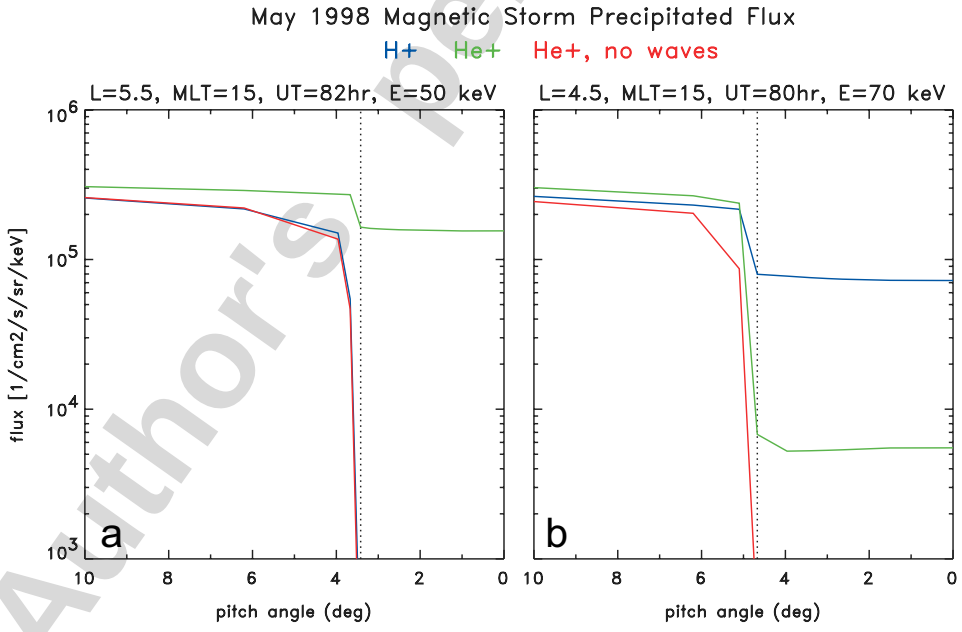

Fig. 3. Pitch-angle distribution functions in the equatorial plane near the main phase of the geomagnetic storm. Two of the strongest pitch-angle diffusion cases are presented. Panel 3(a) represents the event when inequalities (3) and (6) are satisfied at UT = 82 h for an energy of 50 keV, $L = 5.5$, and MLT = 15 for the case of multi-component core plasma. Panel 3(b) illustrates the event when inequalities (3) and (4) are satisfied at UT = 80 h for an energy of 70 keV, $L = 4.5$, and MLT = 15 for the case of electron–proton thermal plasma. The green line in both panels corresponds to the result of RC simulation for the multi-component thermal plasma, the blue line is the case of single-ion thermal plasma, and the red line corresponds to the result when pitch-angle diffusion due to EMIC waves is not included. Only the transition between trapped and loss-cone zones is shown. The vertical lines in the figure correspond to the exact loss cone boundary positions for selected locations.

case of electron–proton thermal plasma simulation. The green line in Fig. 3 corresponds to the result of simulation with the multi-component thermal plasma, the blue line is the case of single-ion thermal plasma, and the red line corresponds to the result when pitch-angle diffusion due to EMIS waves is not included. In order to more clearly illustrate distributions for the strong pitch-angle diffusion events, only the transition between trapped and loss cone zones is shown. The vertical lines in both panels correspond to the exact loss-cone boundary values for selected locations.

As we pointed out before, depending on the stage of the storm, plasma composition, and spatial location, the RC energy range involved in the strong pitch-angle diffusion process is very different. At the selected times and positions presented in Fig. 3, there is no regularity between the multi-component and the single-ion plasma cases that could be used to distinguish the diffusion intensity. Both have very sharp transitions. Although, based on the results presented in Figs. 1 and 2, the transitions between the trapped and loss cone populations are much smoother for most of the strong pitch-angle diffusion events found in the RC-EMIC wave simulation with the heavy thermal ions included. Depending on the magnetospheric plasma content, the spatial locations of EMIC wave excitation can be different, and the results with and without wave induced pitch-angle diffusion would be almost identical as it shown in Fig. 3(a).

Only those RC fluxes that exceed $10^3\,\mathrm{cm}^{-2}\,\mathrm{s}^{-1}\mathrm{st}^{-1}\,\mathrm{keV}^{-1}$ were selected when applying criteria (3)–(6) to the analysis presented above. The inequalities (3)–(6) (and their combinations) are extremely conservative and do not make it possible to see if less intense pitch-angle diffusion is taking place at higher energies. By relaxing these criteria, Fig. 4 shows the pitch angle distributions for energies above 120 keV, missing in previous plots, in comparison with selected low energy RC proton distributions. These results are based on simulation with a multi-component magnetospheric content. The plot presents the pitch-angle distribution function in the equatorial magnetosphere near the main phase of the geomagnetic storm (UT = 82 h) for $L = 5.5$ and MLT = 15. The vertical line corresponds to the exact loss-cone edge for this event. Five different energies, 15, 30, 125, 170, and 235 keV, presented here are involved in the process of strong pitch-angle diffusion. The intensity of pitch-angle diffusion clearly decreases with increasing energy, developing a sharper gradient at the position near the loss cone boundary. The higher the energy of the RC protons, the less intense the interaction between such ions and EMIC waves, while the escape time for high-energy protons is also less. Due to these two facts, we observe in Fig. 4, that the flux transition between the trap zone and loss cone is steeper for higher-energy protons than for the main body of the distribution function. In spite of that, RC ions have a highly isotropic distribution in the loss cone for all presented energies. The only observations near the equatorial plane of proton pitch-angle diffusion related to EMIC waves are those published by Erlandson and Ukhorskiy (2001). However, as has been pointed out by Walt and Voss (2004), "Erlandson and Ukhorskiy (2001) did not observe protons above 17 keV, and the angular distributions of the protons did not reach isotropy as required for strong diffusion". We can only qualitatively compare our calculation with the data presented by Erlandson and Ukhorskiy. In order to do this, we select Example #3 from their paper with the wave activity

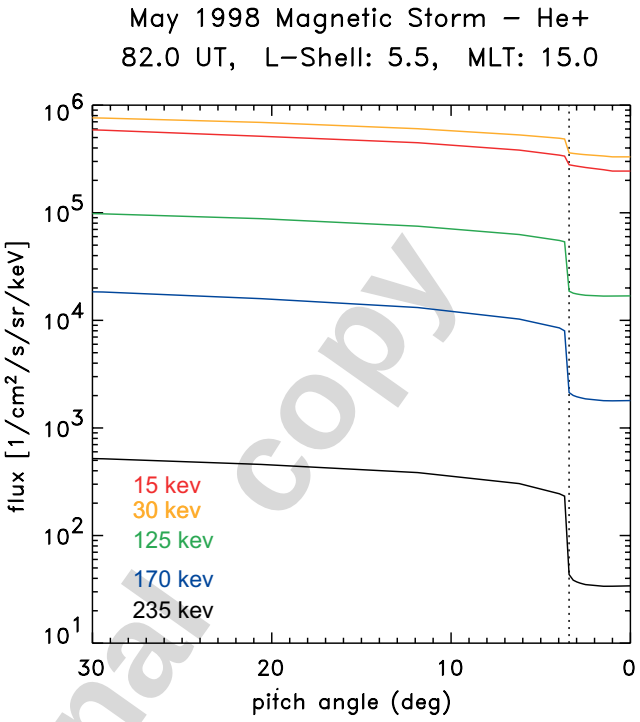

Fig. 4. RC proton pitch-angle distributions for the energies, which are subject to strong pitch-angle diffusion in the case of multi-ion magnetospheric content. There are distributions in the equatorial plane, $L = 5.5$ and MLT = 15, near the main phase of geomagnetic storm, UT = 82 h. The vertical line corresponds to the loss-cone edge. Highly isotropic pith-angle distributions in the loss cone are observed for all energies.

and fluxes observed during the recovery phase of a major magnetic storm (minimum Dst = −110). Indeed, looking at all cases presented above with differing cold plasma magnetospheric content (see Figs. panels 1(a) and 2(a)), only few cases of strong pitch-angle diffusion could be found in the energy range less than 17 keV.

5. Summary and discussion

Do EMIC waves cause strong pitch-angle diffusion of RC ions? This question is the primary motivation of our paper, and from a theoretical point of view the answer is yes. The material presented in the Results section show clear evidence that strong pitch-angle diffusion is taking place in the inner magnetosphere, indicating the important role of the wave–particle interaction mechanism in the distribution of the RC ions and EMIC waves.

The overall distribution and dynamics of strong pitch-angle diffusion events are critically sensitive to many factors. The effects of EMIC waves on RC ion dynamics strongly depend on particle/wave characteristics such as magnetospheric heavy ion content, the ion phase space distribution function, frequency, wave-normal angle, wave energy, and the form of wave spectral energy density. Therefore all of these characteristics should be properly determined by the wave–ion evolution itself. To quantify EMIC wave effects on RC ion dynamics, a self-consistent theoretical description of ions and waves has been employed. This approach has been offered by Khazanov et al. (2002, 2003a). As shown in the previous section, there is a need to couple Eqs. (1) and (2) with a quantitative model that predicts cold, heavy ions magnetospheric content and their dynamics during geomagnetic storms.

The energy precipitation pattern and its spatial location, as well as the intensity of strong pitch-angle diffusion have noticeable differences (see Figs. 1 and 2) depending on the presence of heavy ions in the thermal plasma. There is much stronger pitch-angle diffusion for multi-component (Fig. 1) than for single-ion (Fig. 2) plasmas. The presence of the heavy ions in the magnetosphere also leads to more cases with a flattened transition between the loss cone and trapped regions which is an indication of strong pitch-angle diffusion taking place in the trapped zone.

We have addressed the issue of RC proton strong pitch-angle diffusion and associated EMIC wave generation during different phases of a geomagnetic storm from the theoretical point of view. Additional study is needed to compare our results to exiting strong pitch-angle diffusion data. An example is the self-consistent model of magnetospheric RC interaction with EMIC waves we developed (Khazanov et al., 2002, 2003a, b, 2004a), based on the Volland-Stern (Volland, 1973; Stern, 1975) electric field model, and corresponding to the cold-plasma model of Rasmussen et al. (1993). In a study by Khazanov et al. (2004b), several electric field models were used in conjunction with a RC electron and ion transport model to examine the differences in the net acceleration of particles. It was shown that narrow channels of high electric field are an effective mechanism for injecting plasma into the inner magnetosphere. The Volland–Stern model, which has been used extensively in RC modeling, is shown by Khazanov et al. (2004b), to be incapable of producing flow channels in the electric field distribution. For RC ions, omission of these channels leads to an under estimate of the strength of the storm-time RC and therefore an under estimate of the geoeffectiveness of storm events and the process of strong pitch-angle diffusion development.

Acknowledgments

Funding in support of this study was provided by NASA Grant UPN 370-16-10.

References

Anderson, B.J., Decker, R.B., Paschalidis, N.P., 1997. On the onset of nonadiabatic particle motion in the near-Earth magnetotail. Journal of Geophysical Resarch 102, 17553.

Bespalov, P.A., Trakhtengerts, V.Y., 1986. Cyclotron instability of the Earth radiation belts. In: Leontovich, M.A. (Ed.), Reviews of Plasma Physics, vol. 10. Consultants Bureau, New York, p. 1986.

Blake, J.B., et al., 1995. Comprehensive energetic particle and pitch-angle distribution experiment on POLAR. In: Russell, C.T. (Ed.), The Global Geospace Mission. Kluwer Academic Publishers, Norwell, MA, p. 531.

Braysy, M., Mursula, K., Marklund, G., 1998. Ion cyclotron waves during a great magnetic storm observed by Freja double-probe electric field instrument. Journal of Geophysical Resarch 103, 4145.

Cornwall, J.M., Coroniti, F.V., Thorne, R.M., 1970. Turbulent loss of ring current protons. Journal of Geophysical Resarch 75, 4699.

Erlandson, R.E., Ukhorskiy, A.J., 2001. Observations of electromagnetic ion cyclotron waves during geomagnetic storms: wave occurrence and pitch angle scattering. Journal of Geophysical Resarch 106, 3883.

Farrugia, C.J., et al., 2001. Large-scale geomagnetic effects of 4 May 1998. Adv. Space Res.

Fok, M.-C., Kozyra, J.U., Nagy, A.F., Cravens, T.E., 1991. Lifetime of ring current due to the Coulomb collisions in the plasmasphere. Journal of Geophysical Research 96, 7861.

Gomberoff, L., Neira, R., 1983. Convective growth rate of ion cyclotron waves in H+–He+ and H^+–He^+–O^+ plasma,. Journal of Geophysical Research 88, 2170.

Hauge, R., Soraas, F., 1975. Precipitation of >115 keV protons in the evening and forenoon sectors in relation to magnetic activity. Planetary and Space Science 21, 1141.

Jordanova, V.K., Kistler, L.M., Kozyra, J.U., Khazanov, G.V., Nagy, A.F., 1996. Collisional losses of ring current ions. Journal of Geophysical Research 101, 111.

Jordanova, V.K., Kozyra, J.U., Nagy, A.F., Khazanov, G.V., 1997. Kinetic model of the ring current–atmosphere interactions. Journal of Geophysical Research 102, 14279.

Jordanova, V.K., Farrugia, C.J., Thorne, R.M., Khazanov, G.V., Reeves, G.D., Thomsen, M.F., 2001. Modeling ring current proton precipitation by EMIC waves during the May 14–16, 1997, storm. Journal of Geophysical Research 106, 7–22.

Kennel, C.F., Petschek, H.E., 1966. Limit on stably trapped particle fluxes. Journal of Geophysical Research 71, 1.

Khazanov, G.V., Gamayunov, K.V., Jordanova, V.K., Krivorutsky, E.N., 2002. A self-consistent model of the interacting ring current ions with electromagnetic ICWs. Initial results: waves and precipitating fluxes. Journal of Geophysical Research 107, 6.

Khazanov, G.V., Gamayunov, K.V., Jordanova, V.K., 2003a. Self-consistent model of magnetospheric ring current ions and electromagnetic ion cyclotron waves: the 2–7 May 1998 storm. Journal of Geophysical Research 108.

Khazanov, G.V., Liemohn, M.W., Newman, T.S., Fok, M.-C., Spiro, R.W., 2003b. Self-consistent magnetosphere–ionosphere coupling: theoretical studies. Journal of Geophysical Research 108.

Khazanov, G.V., Krivorutsky, E.N., Gamayunov, K.V., Avanov, L.A., 2004a. The nonlinear coupling of electromagnetic ion cyclotron and lower hybrid waves in the ring current region: the magnetic storm May 1–7 1998. Nonlinear Processes in Geophysics 11, 229–239.

Khazanov, G.V., Liemohn, M.W., Newman, T.S., Fok, M.-C., Ridley, A., 2004b. Magnetospheric convection electric field dynamics and stormtime particle energization: case study of the magnetic storm of May 4, 1998. Annales de Geophysique 22, 497–510.

Kozyra, J.U., Cravens, T.E., Nagy, A.F., Fontheim, E.G., Ong, R.S.B., 1984. Effect of energetic heavy ions on electromagnetic ion cyclotron wave generation in the plasmapause region. Journal of Geophysical Research 89, 2217.

Kozyra, J.U., Fok, M.-C., Sanchez, E.R., Evans, D.S., Hamilton, D.C., Nagy, A.F., 1998. The role of precipitation losses in producing the rapid early recovery phase of the Great Magnetic Storm of February 1986. Journal of Geophysical Research 103, 6801.

Liemohn, M.W., Kozyra, J.U., Jordanova, V.K., Khazanov, G.V., Thomsen, M.F., Cayton, T.E., 1999. Analysis of early phase ring current recovery mechanisms during geomagnetic storms. Geophysical Research Letters 26, 2845–2848.

Lyons, L.R., Williams, D.J., 1984. Quantitative Aspects of Magnetospheric Physics. Reidel, Dordrecht.

O'Brien, B.J., 1964. High-latitude geophysical studies with satellite Injune 3. Precipitation of electrons into the atmosphere. Journal of Geophysical Research 69, 13.

Rasmussen, C.E., Guiter, S.M., Thomas, S.G., 1993. Two-dimensional model of the plasmasphere: refilling time constants. Planetary and Space Science 41, 35.

Schulz, M., Lanzerotti, L.J., 1974. Particle Diffusion in the Radiation Belts. Springer, New York.

Sergeev, V.A., Sazhina, E.M., Tsyganenko, N.A., Lundblad, J.A., Soraas, F., 1983. Pith angle scattering of energetic protons in the magnetotail current sheet as the dominant source of their isotropic precipitation into the nightside ionosphere. Planetary and Space Science 31, 1147.

Smith, P.H., Hoffman, R.A., Fritz, T.A., 1976. Ring current proton decay is charge exchange. Journal of Geophysical Research 81, 2701.

Soraas, F., Aarsnes, K., Lundblad, J.A., Evans, D.S., 1999. Enhanced pitch angle scattering of protons at mid-latitude during geomagnetic storms. Physics and Chemistry of the Earth, Part C 24, 287.

Stern, D.P., 1975. The motion of a proton in the equatorial magnetosphere. Journal of Geophysical Research 80, 595.

Volland, H., 1973. A semiempirical model of large-scale magnetospheric electric fields. Journal of Geophysical Research 78, 171.

Walt, M., Voss, H.D., 2001. Losses of ring current ions by strong pitch angle scattering. Geophysical Research Letters 24, 3839.

Walt, M., Voss, H.D., 2004. Proton precipitation during magnetic storms in August through November 1998. Journal of Geophysical Research 109, 6.

Yahnina, T.A., Yahnin, A.G., Kangas, J., Manninen, J., 2000. Proton precipitation related to Pc 1 pulsations. Geophysical Research Letters 27, 3575.

Young, D.T., Balsiger, H., Geiss, J., 1982. Correlations of magnetospheric ion composition with geomagnetic and solar activity. Journal of Geophysical Research 87, 9077–9096.